Bioconjugate Chemistry

Article

pubs.acs.org/bc

# Novel Pullulan Bioconjugate for Selective Breast Cancer Bone Metastases Treatment

Gwénaëlle Bonzi,[†] Stefano Salmaso,[†] Anna Scomparin,[‡] Anat Eldar-Boock,[‡] Ronit Satchi-Fainaro,[‡] and Paolo Caliceti*[,†]

[†]Department of Pharmaceutical and Pharmacological Sciences, University of Padua, Via F. Marzolo 5, 35131 Padua, Italy

[‡]Department of Physiology and Pharmacology, Sackler School of Medicine, Tel Aviv University, Tel Aviv 69978, Israel

Supporting Information

**ABSTRACT:** A novel polysaccharide bioconjugate was designed to selectively target breast cancer bone metastases using a bisphosphonate moiety (alendronate, ALN). Paclitaxel (PTX) was first covalently conjugated to pullulan (Pull) through a Cathepsin K-sensitive tetrapeptide spacer followed by a self-immolative aminobenzyl alcohol spacer to obtain Pull-(GGPNle-$\varphi$-PTX). ALN was then conjugated to the polymeric backbone of Pull-(GGPNle-$\varphi$-PTX) via a PEG spacer. The final bioconjugate Pull-(GGPNle-$\varphi$-PTX)-(PEG-ALN) was found to assemble into colloidal spherical structures, which were physically and chemically stable under physiological conditions. In vitro studies showed that Pull-(GGPNle-$\varphi$-PTX)-(PEG-ALN) had strong affinity for hydroxyapatite, which simulates the bone tissue. Paclitaxel was rapidly released from the bioconjugate by Cathepsin K cleavage under pathological conditions. All studies performed using human MDA-MB-231-BM (bone metastases-originated clone), murine 4T1 breast cancer cells, murine K7M2, and human SAOS-2 osteosarcoma cells showed that the bioconjugate exerted an enhanced antiproliferative activity compared to the conjugate without the ALN. Furthermore, the nanoconjugate inhibited the migration of cancer cells and further displayed potent anti-angiogenic activity. In conclusion, the results showed that this conjugate has an excellent potential for selective treatment of bone neoplasms such as breast cancer bone metastases and osteosarcoma.

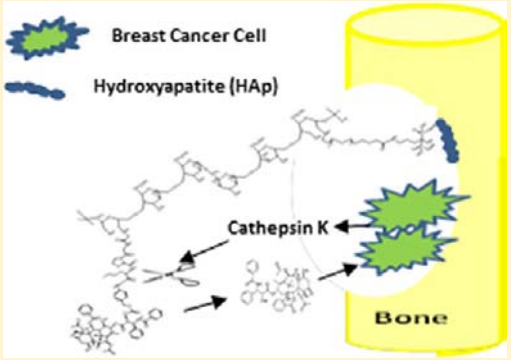


## 1. INTRODUCTION

One of the major causes of cancer-related death among women worldwide is the development of bone metastases affecting about 70−80% of late stage breast cancer patients.[1,2] Furthermore, bone metastases deteriorate the skeletal health and bone integrity of these patients, which worsens their clinical conditions and quality of life.[3]

In order to reduce bone resorption and tumor progression in patients with metastases originating from primary breast cancer, bisphosphonates have been combined with anticancer drugs.[4−7] Bisphosphonates have in fact high affinity for hydroxyapatite (HAp) bone mineral surfaces with a preference for active metabolic sites of osteolysis formed during tumor development. As a result, bisphosphonates inhibit the dissolution of hydroxyapatite crystals of the bone matrix. Furthermore, nitrogen-containing bisphosphonates, namely, alendronate, have been found to be adsorbed by osteoclasts via endocytosis during bone resorption and inhibit the farnesyl pyrophosphate (FPP) synthase, an enzyme involved in the mevalonate pathway. The inhibition of this enzyme prevents the biosynthesis of isoprenoid lipids (FPP and GGPP), which are essential for the post-translational farnesylation and geranylgeranylation of small GTPase signaling proteins. The later inhibits osteoclast activity, reduces bone resorption, and turnover and induces apoptosis.[8,9] Accordingly, bisphosphonates associated with paclitaxel have been found to display a synergistic cytotoxic effect toward breast cancer cells, thus introducting a new perspective in combination therapies.[9]

Paclitaxel is an antimitotic drug approved for the treatment of ovarian, breast, and non-small cell lung cancer at late stage.[10] Due to its low solubility and stability in water, the clinically used product Taxol is formulated as a mixture of Cremophor EL and ethanol, which is responsible for dose-limiting toxicity, namely, hypersensitivity and neuropathy.[11] The poor selectivity toward tumors, often associated with damage to normal healthy cells, represents an additional drawback to the use of this drug.

So far, various colloidal delivery systems have been investigated to enhance the pharmaceutical performance of paclitaxel. Liposomes, micelles, nanoparticles, and polymer bioconjugates have been developed to increase the drug solubility and stability, prolong the permanence in the bloodstream, favor the accumulation into tumor tissues via passive mechanisms, namely, enhanced permeability and retention (EPR) effect, selectively target the tumor cells, and finally release the drug into the extracellular matrix or in the intracellular compartments.[12] Polymer therapeutics based on

**Received:** December 23, 2014
**Revised:** January 22, 2015
**Published:** January 22, 2015

  

DOI: 10.1021/bc500614b
*Bioconjugate Chem.* 2015, 26, 489−501

Scheme 1. Chemical Structure of Pull-(GGPNle-$\varphi$-PTX)-(PEG-ALN)

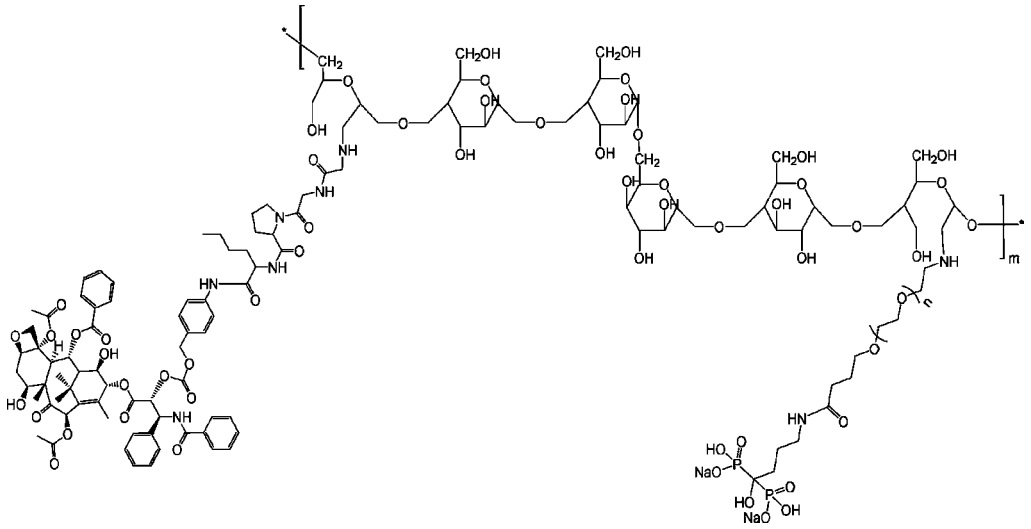

*N*-(2-hydroxypropyl)methacrylamide (HPMA),[12,13] polyamidoamine and poly(ethylene glycol) (PEG) copolymers,[6] polyglutamic acid in preclinical investigations[14] and in clinical trials (Opaxio),[15] and the FDA-approved albumin nanoparticle (Abraxane)[16] are a few examples of colloidal formulations that have successfully enhanced the biopharmaceutical and pharmacokinetic properties of paclitaxel as well as its accumulation in the tumor tissue and therapeutic performance.

Polymer bioconjugates bearing both bisphosphonates and anticancer drugs have been investigated to synergistically combine the antimitotic effect of paclitaxel with the bone targeting and anti-angiogenic properties of bisphosphonates.[4,9,17,18] Typical examples are PEG-based dendrimers and HPMA copolymers derivatized with paclitaxel and alendronate that, in vitro and in vivo, have been found to yield selective treatment of breast cancer bone metastasis.[19,20]

Natural and semisynthetic polysaccharides, namely, dextran, chitosan, hyaluronic acid, and pullulan, are excellent platforms to produce anticancer polymer therapeutics for combined drug delivery.[21] Indeed, these biodegradable and multivalent polymers can be derivatized with multiple copies of drugs and targeting agents.[7,18,22] Pullulan, in particular, is an attractive and versatile candidate for numerous biomedical applications, namely, drug delivery and tissue engineering.[23] The maltotriose structure of this natural polysaccharide can be chemically modified to produce derivatives with unique physicochemical properties. Pullulan based colloidal systems for the delivery of anticancer drugs include self-assembling hydrophobized pullulan,[24] pH-sensitive pullulan nanoparticles,[16] and pullulan bioconjugates.[25,26] Bioconjugates have also been designed for active tumor targeting. A pullulan derivative bearing doxorubicin and folic acid has shown high selectivity for tumor cells that overexpress the folic acid receptor.[14,27]

Although several polysaccharide-based systems are under development for anticancer drug delivery, to the best of our knowledge, none of them has been designed for the treatment of breast cancer bone metastases.

In order to exploit the peculiar physicochemical properties of pullulan to produce an efficient system for the treatment of breast cancer bone metastases, a novel polymer bioconjugate bearing paclitaxel and alendronate attached to the polysaccharide backbone has been designed. Alendronate was used as targeting agent as it binds the hydroxyapatite (HAp) that is progressively exposed at osteolytic lesions and site of active bone resorption induced by the breast cancer metastasis.[22] Paclitaxel, the drug of choice for treatment of breast cancer cells, was attached to the polymer through a cathepsin K-cleavable peptide that selectively releases the drug at the tumor site. Cathepsin K is in fact overexpressed by breast cancer cells and secreted at the osteoclast resorption lacunae (Howship's lacunae) formed by the metastasis.[28]

The synthesis as well as biopharmaceutical and pharmacodynamic characterization of the novel bioconjugate are reported here.

## 2. RESULTS

The chemical structure of Pull-(GGPNle-$\varphi$-PTX)-(PEG-ALN) is reported in Scheme 1. The structures of the two reference bioconjugates, Pull-(GGPNle-$\varphi$-PTX)-(PEG-COOH) and Pull-(PEG-ALN), are reported in Scheme SI1 of Supporting Information (SI).

**2.1. Synthesis and Physicochemical Characterization of Pull-(GGPNle-$\varphi$-PTX)-(PEG-COOH), Pull-(PEG-ALN) and Pull-(GGPNle-$\varphi$-PTX)-(PEG-ALN).** In order to conjugate PTX and ALN to Pull, the polysaccharide backbone was activated by selective periodate oxidation. The potentiometric analyses revealed 44 aldehyde groups out of 100 glucose units. However, as a result of the spontaneous hemiacetal formation,[29] only 2/3 of aldehydes could be detected. Therefore, the periodate oxidation generated 66 aldehydes out of 100 glucose units corresponding to 33% oxidized glucose units, which fairly fitted the theoretical oxidation end-point.

The GPC analyses showed that the Pull oxidation reduced the polysaccharide molecular weight from 110 kDa to approximately 89 kDa and the polydispersity index (PDI, $M_w/M_n$) from 2.35 to 1.88.

The anticancer drug module $NH_2$GlyGlyProNLE-$\varphi$-PTX was obtained through a 5-step protocol described in SI Scheme SI2. The intermediates were characterized by mass spectrometry and $^1$H NMR (SI Figures SI1−SI5). The purity of the final product, evaluated by RP-HPLC, was >95% (SI Figure SI6) and the product yield was 30% mol of tetrapeptide.

The synthesis of the targeting module $NH_2$PEG-ALN (SI Scheme SI3) resulted in 25% mol PEG derivatization with



DOI: 10.1021/bc500614b
Bioconjugate Chem. 2015, 26, 489−501

**Table 1. Composition and Calculated Molecular Weight of Pull-(GGPNle-φ-PTX)-(PEG-ALN), Pull-(GGPNle-φ-PTX)-(PEG-COOH), and Pull-(PEG-ALN) Bioconjugates[a]**

| | Pull-(GGPNle-φ-PTX)-(PEG-ALN) | | Pull-(GGPNle-φ-PTX)-(PEG-COOH) | | Pull-(PEG-ALN) | |
|---|---|---|---|---|---|---|
| | % w/w[b] | derivatized aldehydes (%mol) | % w/w[b] | derivatized aldehydes (%mol) | % w/w[b] | derivatized aldehydes (%mol) |
| PTX | 7.8 | 12.4 | 8.1 | 10.9 | - | - |
| ALN | 1.6 | 6.7 | - | - | 2.0 | 5.3 |
| PEG-COOH | 44.3 | 20.1 | 60 | 23.0 | 55.4 | 15.9 |
| Pull | 27.2 | - | 31.9 | - | 42.6 | - |
| Mol wt (kDa) | 329 | - | 292 | - | 248 | - |

[a]% w/w content of conjugated PTX, ALN, and PEG-COOH in the final products and % of derivatized aldehydes with PTX, ALN, and PEG-COOH. [b]% w/w was calculated as the amounts of the single components in the final products. The PTX and ALN contents were calculated without spacers.

ALN. The trifluoroacetic acid treatment of tBoc-PEG-ALN yielded 100% terminal amino group deprotection without ALN release.

Pull-(GGPNle-φ-PTX)-(PEG-ALN) and Pull-(GGPNle-φ-PTX)-(PEG-COOH) were obtained by sequential derivatization of the aldehyde groups of the oxidized pullulan with (1) $NH_2$GlyGlyProNle-φ-PTX and (2) $NH_2$PEG-ALN or $NH_2$PEG-COOH (SI Scheme SI4). The conjugation reaction was carried out by reductive amination. The conjugation of $NH_2$GlyGlyProNle-φ-PTX was carried out using sodium triacetoxyborohydride, which selectively reduces the Schiff bases to amino groups. The conjugation of $NH_2$PEG-ALN or $NH_2$PEG-COOH to the residual aldehyde groups of Pull-(GGPNle-φ-PTX) was carried out using sodium borohydride, which reduces both Schiff bases to amino groups and unreacted aldehydes to alcohols. Pull-(PEG-ALN) was obtained by direct $NH_2$-PEG-ALN conjugation to the oxidized pullulan and final reduction with sodium borohydride.

The composition and the molecular weight of the bioconjugates reported in Table 1 were calculated by chromatographic and spectrometric analyses of the intermediate and final products.

The RP-HPLC analyses revealed that after purification the content of free PTX in the Pull-(GGPNle-φ-PTX)-(PEG-ALN) product was below 0.3% (free PTX/total PTX, %, SI Figure SI7). A similar result was obtained with Pull-(GGPNle-φ-PTX)-(PEG-COOH). The free ALN content in the Pull-(GGPNle-φ-PTX)-(PEG-ALN) and Pull-(PEG-ALN) product evaluated by spectrophotometric analysis was below the detection limit.

The solubility of Pull-(GGPNle-φ-PTX)-(PEG-ALN) was 6.6 mg/mL, which corresponds to 513 μg/mL PTX-equivalent, 1700 times higher than the free drug solubility (0.3 μg/mL).[30]

The morphological and dimensional features of Pull-(GGPNle-φ-PTX)-(PEG-ALN) were examined by transmission electron microscopy (TEM) and by dynamic light scattering (DLS) at pH 5.5, corresponding to the pH of the osteoclast lacunae, pH 6.5 (water) and pH 7.4, corresponding to the pH of the blood.

The TEM images reported in Figure 1 (insert) show that under physiological conditions the bioconjugate forms spheroidal structures. The DLS data showed that the hydrodynamic diameter and size polydispersity (PDI) at pH 5.5, 6.5, and pH 7.4 (SI Figure SI8) were 163.3 ± 18.3 nm (PDI 0.20 ± 0.02), 108.4 ± 6.9 nm (PDI 0.17 ± 0.03), and 69.9 ± 6.3 (PDI 0.15 ± 0.01), respectively. We show that the size of the colloidal dispersions were fairly stable over 8 h (Figure 1). In all cases, PTX concentration in the solutions did not decrease over the experimental time.

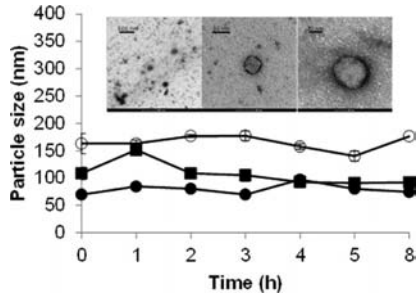


**Figure 1.** TEM images of Pull-(GGPNle-φ-PTX)-(PEG-ALN) in PBS, pH 7.4, and dimensional time course profiles of Pull-(GGPNle-φ-PTX)-(PEG-ALN) size in PBS, pH 5.5 (○); water, pH 6.5 (■); PBS, pH 7.4 (●).

The critical micellar concentration (CMC) of Pull-(GGPNle-φ-PTX)-(PEG-ALN) determined by fluorescence analysis (SI Figure SI9) was 73.3 μg/mL, which was below 0.5 μM. Similar results were obtained with Pull-(GGPNle-φ-PTX)-(PEG-COOH) while Pull-(PEG-ALN) did not reach a CMC.

**2.2. Pull-(GGPNle-φ-PTX)-(PEG-ALN) Possesses Targeting Properties and Selective Drug Release.** The bone affinity of Pull-(GGPNle-φ-PTX)-(PEG-ALN) was assessed by using hydroxyapatite (HAp) as a bone tissue model.[4,31] Free ALN and Pull-(GGPNle-φ-PTX)-(PEG-COOH) were used as positive and negative references, respectively.

Here we show the binding profiles obtained at pH 5.5 (Figure 2A) and 7.4 (Figure 2B). The binding of ALN to HAp was not affected by the pH. After 5 min incubation, about 72% of free ALN was bound to HAp and a plateau corresponding to 80% binding was achieved in 3 h. The binding of Pull-(GGPNle-φ-PTX)-(PEG-COOH) to HAp was negligible at both pH. On the contrary, Pull-(GGPNle-φ-PTX)-(PEG-ALN) displayed pH-dependent affinity for HAp and, in contrast to ALN, the bioconjugate interaction was not immediate. At pH 5.5, the interaction of Pull-(GGPNle-φ-PTX)-(PEG-ALN) with HAp progressively increased throughout time to reach maximal binding of about 60% in 3 h. At pH 7.4, about 30% of binding was achieved within 2 h, and then, it further slowly increased to yield about 40% binding in 8 h.

The PTX release from Pull-(GGPNle-φ-PTX)-(PEG-ALN) and Pull-(GGPNle-φ-PTX)-(PEG-COOH) was evaluated at pH 5.5 and pH 7.4, at 37 °C, either in the absence or in the presence of Cathepsin K. In the absence of Cathepsin K, at both pHs, PTX was not released from the bioconjugates throughout the experimental time.

We show that in the presence of Cathepsin K at pH 7.4, PTX was not released, while at pH 5.5 about 50% of PTX was



DOI: 10.1021/bc500614b
Bioconjugate Chem. 2015, 26, 489−501

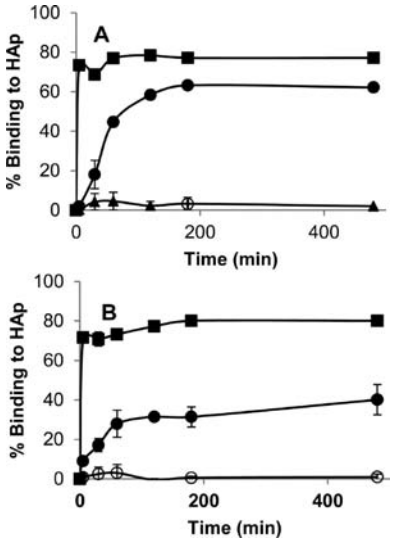


**Figure 2.** HAp binding profiles of ALN (■), Pull-(GGPNle-φ-PTX)-(PEG-ALN) (●), Pull-(GGPNle-φ-PTX)-(PEG-COOH) (○). (A) pH 5.5 and (B) pH 7.4.

released in 35 min and over 96% of the drug was released in 7 h (Figure 3). It is worth noting that no differences were observed in PTX release from Pull-(GGPNle-φ-PTX)-(PEG-ALN) and Pull-(GGPNle-φ-PTX)-(PEG-COOH) (data not shown).

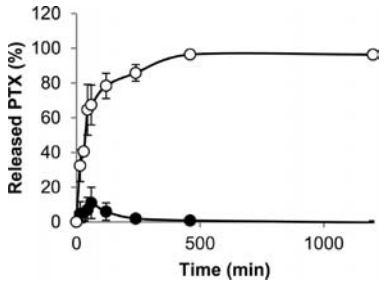


**Figure 3.** PTX release profiles from Pull-(GGPNle-φ-PTX)-(PEG-ALN) incubated at pH 5.5 in the presence of Cathepsin K (○) and in the absence of Cathepsin K (●).

**2.3. Pullulan Conjugates Do Not Cause RBC Lysis.** Hemocompatibility studies were carried out by incubating rat red blood cells (RBC) with Pull-(GGPNle-φ-PTX)-(PEG-ALN) or equivalent PTX and ALN amounts in 1:1:8 ethanol/Cremophor EL. Dextran and poly(ethylene imine) (PEI) were also tested as negative and positive control for hemolysis, respectively.[32,33]

The hemolytic profiles reported in Figure 4 show that, similarly to dextran, Pull-(GGPNle-φ-PTX)-(PEG-ALN) induces negligible hemolysis up to 5 mg/mL while the PTX and ALN mixture in 1:1:8 ethanol/Cremophor EL induced slight hemolysis as compared to the positive control PEI.

**2.4. Pullulan Conjugates Maintain in Vitro Paclitaxel Cytotoxicity and Anti-Angiogenic Properties on Several Cancer Cell Lines.** The cytotoxic activity of Pull-(GGPNle-φ-PTX)-(PEG-ALN) was examined by using human mammary bone metastasis MDA-MB-231-BM, murine mammary adenocarcinoma 4T1, osteosarcoma K7M2, and osteosarcoma SAOS-2 cell lines. ALN- and PTX-equivalent concentrations of Pull-(GGPNle-φ-PTX)-(PEG-ALN), Pull-(GGPNle-φ-PTX)-(PEG-COOH), Pull-(PEG-ALN), free ALN, and free PTX were comparatively tested.

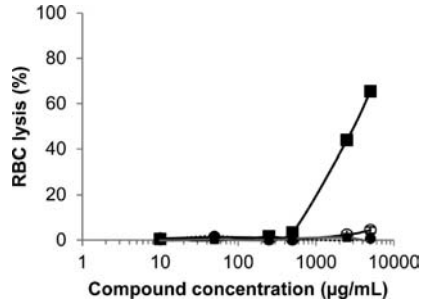


**Figure 4.** Hemocompatibility profiles obtained by RBC incubation with PTX+ALN in Cremofor EL (○), Pull-(GGPNle-φ-PTX)-(PEG-ALN) (●), Dextran (×), and PEI (■).

The cell viability profiles reported in Figure 5 show that the cell proliferation was inhibited by both Pull-(GGPNle-φ-PTX)-(PEG-ALN) and Pull-(GGPNle-φ-PTX)-(PEG-COOH). The data reported in Table 2 show that, with the exception of K7M2 cells, the $IC_{50}$ obtained with Pull-(GGPNle-φ-PTX)-(PEG-ALN) was about 5−20 times higher than that obtained with PTX and the $IC_{50}$ of Pull-(GGPNle-φ-PTX)-(PEG-COOH) was about 5−10-fold higher as compared to Pull-(GGPNle-φ-PTX)-(PEG-ALN). In the case of K7M2 cells, Pull-(GGPNle-φ-PTX)-(PEG-ALN) was 5 times more active than PTX and 30 times more active than Pull-(GGPNle-φ-PTX)-(PEG-COOH). Pull, ALN, and Pull-(PEG-ALN) were not toxic even at very high concentration.

**2.5. Pullulan Conjugates Inhibit the Migration of Breast Cancer Cells in a Wound Healing-Like Assay.** The migration of MDA-MB-231-BM cells, which model the breast cancer metastasis, was examined by 24 h cell incubation with Pull-(GGPNle-φ-PTX)-(PEG-ALN), Pull-(GGPNle-φ-PTX)-(PEG-COOH), Pull-(PEG-ALN), free PTX, free ALN, a combination of free ALN and free PTX, and Pull. The study was carried out using equivalent Pull, PTX, and ALN concentrations.

The results reported in Figure 6 show that ALN, Pull, and Pull-(PEG-ALN) have no effect on the MDA-MB-231-BM migration. PTX and the PTX/ALN mixture yielded a similar migration inhibition effect while Pull-(GGPNle-φ-PTX)-(PEG-COOH) and Pull-(GGPNle-φ-PTX)-(PEG-ALN) inhibited the migration of MDA-MB-231-BM of about 80−85% of initial gap as compared with a 100% inhibition obtained with free PTX.

The enlarged images of the cells after 24 h treatment (SI Figure SI10) showed a difference in the cell morphology due to cell death, as both paclitaxel and alendronate have been proven to be anti-tumorogenic drugs. Therefore, it was expected that paclitaxel and alendronate affect tumor cell morphology and function as previously observed.[34]

**2.6. Pullulan Conjugates Maintain and Increase PTX Anti-Angiogenic Properties on Human Umbilical Vein Endothelial Cells (HUVEC).** The anti-angiogenic activity of Pull-(GGPNle-φ-PTX)-(PEG-ALN) was evaluated by determining the cytotoxic effect on human umbilical vein endothelial cells (HUVEC) and by capillary-like tube formation assay performed on Matrigel. The comparative study was performed using Pull-(GGPNle-φ-PTX)-(PEG-ALN), Pull-(GGPNle-φ-PTX)-(PEG-COOH), Pull-(PEG-ALN), PTX, ALN, Pull, and at PTX- and ALN-equivalent concentrations.


DOI: 10.1021/bc500614b
Bioconjugate Chem. 2015, 26, 489−501

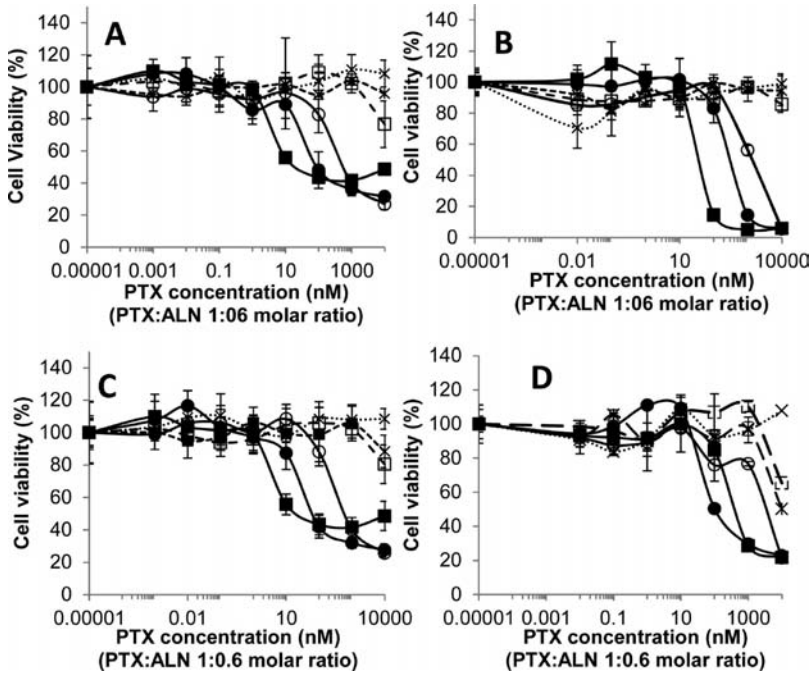


**Figure 5.** Cell toxicity of PTX (■), Pull-(GGPNle-φ-PTX)-(PEG-ALN) (●), and Pull-(GGPNle-φ-PTX)-(PEG-COOH) (○). The ALN concentrations in the free ALN (★) and Pull-(PEG-ALN) (□) solutions are equivalent to the ALN concentrations of the Pull-(GGPNle-φ-PTX)-(PEG-ALN) (▲) solution. The Pull concentrations (×) are equivalent to the Pull concentrations of Pull-(GGPNle-φ-PTX)-(PEG-ALN). (A) MDA-MB-231-BM human mammary adenocarcinoma cells from bone metastasis; (B) murine mammary adenocarcinoma 4T1 cells; (C) human osteosarcoma SAOS-2 cells; (D) murine osteosarcoma K7M2 cells. The data represent the mean ± SD (standard deviation) calculated from 3 independent experiments done in triplicates each.

**Table 2. Cytoxicity Activity of PTX, Pull-(GGPNle-φ-PTX)-(PEG-ALN), and Pull-(GGPNle-φ-PTX)-(COOH)**

| | $IC_{50}$ (nM) | | | |
|---|---|---|---|---|
| | 4T1 | SAOS-2 | K7M2 | MDA-MB-231-BM |
| PTX | 30 | 3 | 500 | 20 |
| Pull-(GGPNle-φ-PTX)-(PEG-ALN) | 300 | 60 | 100 | 90 |
| Pull-(GGPNle-φ-PTX)-(PEG-COOH) | 1500 | 500 | 3000 | 500 |

We show that 72 h cell incubation with free PTX and Pull-(GGPNle-φ-PTX)-(PEG-ALN) yielded similar HUVEC proliferation inhibition with $IC_{50}$ of about 15 nM (Figure 7). Pull-(GGPNle-φ-PTX)-(PEG-COOH) was less cytotoxic than Pull-(GGPNle-φ-PTX)-(PEG-ALN) and exhibited an $IC_{50}$ of about 700 nM.

The capillary-like tube formation assay performed on Matrigel was carried out under non-cytotoxic conditions, which were preliminarily determined for each tested sample.

We show that Pull-(GGPNle-φ-PTX)-(PEG-COOH) and Pull-(GGPNle-φ-PTX)-(PEG-ALN) displayed significant anti-angiogenic activity (Figure 8; enlarged images of panel A SI Figure SI11). Similarly to PTX alone or in combination with ALN, both conjugates inhibited the formation of tubular structures of HUVEC by about 60%, while Pull and ALN, either free or polymer-conjugated, did not affect the formation of capillary-like tubes.

**2.7. Wound Healing Assays.** The migration of HUVEC, was evaluated by 13 h cell incubation with Pull-(GGPNle-φ-PTX)-(PEG-ALN), Pull-(GGPNle-φ-PTX)-(PEG-COOH), Pull-(PEG-ALN), free PTX, free ALN, a combination of free ALN and free PTX, and Pull. The comparative study was carried out using equivalent Pull, PTX, and ALN concentrations.

The results reported in Figure 9 show that ALN, Pull, and Pull-(PEG-ALN) have no effect on the HUVEC migration inhibition. PTX and Pull-(GGPNle-φ-PTX)-(PEG-COOH) yielded similar migration inhibition effect, while the PTX/ALN mixture and Pull-(GGPNle-φ-PTX)-(PEG-ALN) inhibited the migration of HUVEC at about 70% of the initial gap as compared to 100% inhibition obtained with free PTX.

Similarly to what was reported above for migration of MDA-MB-231-BM cells, the enlarged images of the cells after 13 h treatment (Figure SI12) showed a difference also in endothelial cell morphology due to the dual effect of paclitaxel and alendronate, both anti-tumorogenic and anti-angiogenic effects.[19]

## 3. DISCUSSION

The Pull-(GGPNle-φ-PTX)-(PEG-ALN) conjugate was designed to yield selective tumor accumulation and paclitaxel (PTX) release in the bone lacunae formed by breast cancer metastasis. According to its colloidal size, the conjugate can passively accumulate by EPR effect while alendronate (ALN), which interacts with hydroxyapatite (HAp) exposed in the bone lacunae,[22] provides for the permanence in these sites.

ALN was conjugated to the pullulan (Pull) backbone through a PEG chain (PEG-ALN) to enhance the ALN exposure for the recognition of and interaction with the bone matrix. Paclitaxel (PTX) was attached to the polymer backbone through the Cathepsin K-sensitive linker Gly-Gly-Pro-Nle tetrapeptide (GGPNle).[25] This enzyme is overexpressed by cancer cells and secreted to the bone lacunae where it is involved in the osteoclast resorption.[28] The 4-aminobenzyl


DOI: 10.1021/bc500614b
Bioconjugate Chem. 2015, 26, 489−501

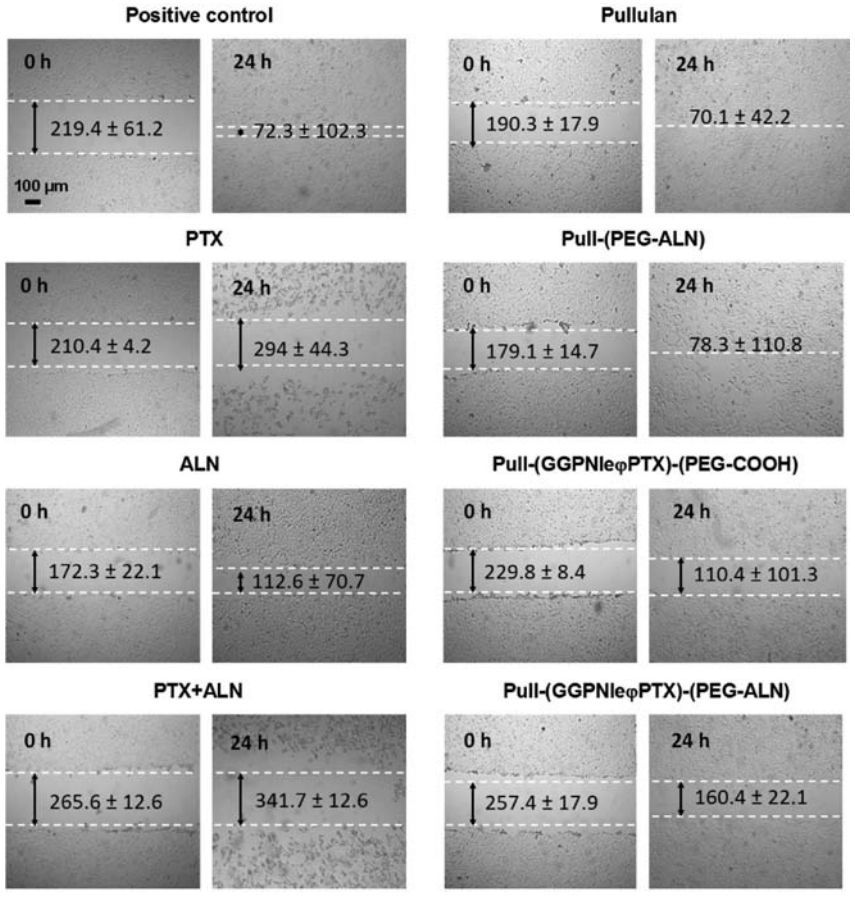


**Figure 6.** Wound healing assay on MDA-MB-231-BM cells incubated with free PTX, free ALN, Pull, Pull-(GGPNle-$\varphi$-PTX)-(PEG-COOH), Pull-(PEG-ALN), and Pull-(GGPNle-$\varphi$-PTX)-(PEG-ALN) at equivalent concentration of PTX for 24 h.

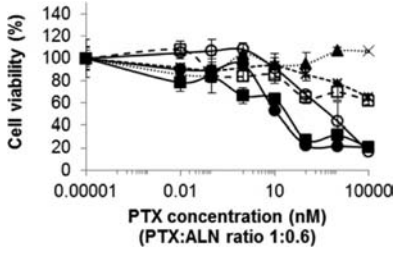


**Figure 7.** Cytotoxicity assay on human umbilical vein endothelial cell (HUVEC). HUVEC were incubated with free PTX (■), free ALN (★), Pull (×), Pull-(GGPNle-$\varphi$-PTX)-(PEG-COOH) (○), Pull-(PEG-ALN) (□), and Pull-(GGPNle-$\varphi$-PTX)-(PEG-ALN) (●) at equivalent concentration of PTX and ALN for 72 h. Data represent the mean ± SD (standard deviation).

alcohol moiety ($\varphi$) was introduced to overcome steric limitations between GGPNle and PTX.[35,36]

The Pull activation was carried out by selective periodate oxidation of the vicinal diols, which generates reactive aldehyde groups along the polysaccharide backbone that can be properly derivatized with multiple copies of drug and targeting agents. The oxidation degree was selected in order to attach 5−10 PTX molecules out of 100 glucose units, which was considered a suitable degree of derivatization to balance the drug payload with the biopharmaceutical properties of the bioconjugate, namely, solubility and homogeneity. Preliminary studies showed in fact that the bioconjugate solubility decreases and the formation of heterogeneous aggregates increases as the number of PTX molecules attached to the polymer backbone increases (data not shown).

The synthesis process endowed a derivative [Pull-(GGPNle-$\varphi$-PTX)-(PEG-ALN)] bearing about 6 PTX, 3 ALN, and 9 PEG-COOH molecules out of 100 glucose units, corresponding to the overall derivatization of about 40% of the reactive aldehyde groups. Similar aldehyde derivatization degree was obtained in the case of Pull-(GGPNle-$\varphi$-PTX)-(PEG-COOH) suggesting that steric hindrance phenomena limit the complete derivatization of the aldehyde groups. Considering that the oxidation produces two aldehyde groups in the same glucose unit, the results seem to indicate that only one aldehyde per glucose unit is sterically available for conjugation. Since aldehydes may form covalent adducts with nucleophilic functions of biological macromolecules, namely, proteins, resulting in toxic effects,[37] a final reduction of the bioconjugates with sodium borohydride was carried out to quench the unreacted aldehydes. The opposite of sodium triacetoxyborohydride, which selectively reduces the Schiff's bases,[38] sodium borohydride extensively reduces both Schiff's bases to amino groups and aldehyde groups to alcohols.[39] Validation studies performed with oxidized pullulan showed that aldehydes along the backbone were efficiently quenched by reaction with sodium borohydride (data not shown).

Critical micellar concentration (CMC), dynamic light scattering (DLS), and transmission electron microscopy (TEM) analyses were carried out to elucidate the physical properties of the bioconjugate in solution, namely, morphology, self-assembly, and size, which are known to be critical in


DOI: 10.1021/bc500614b
Bioconjugate Chem. 2015, 26, 489−501

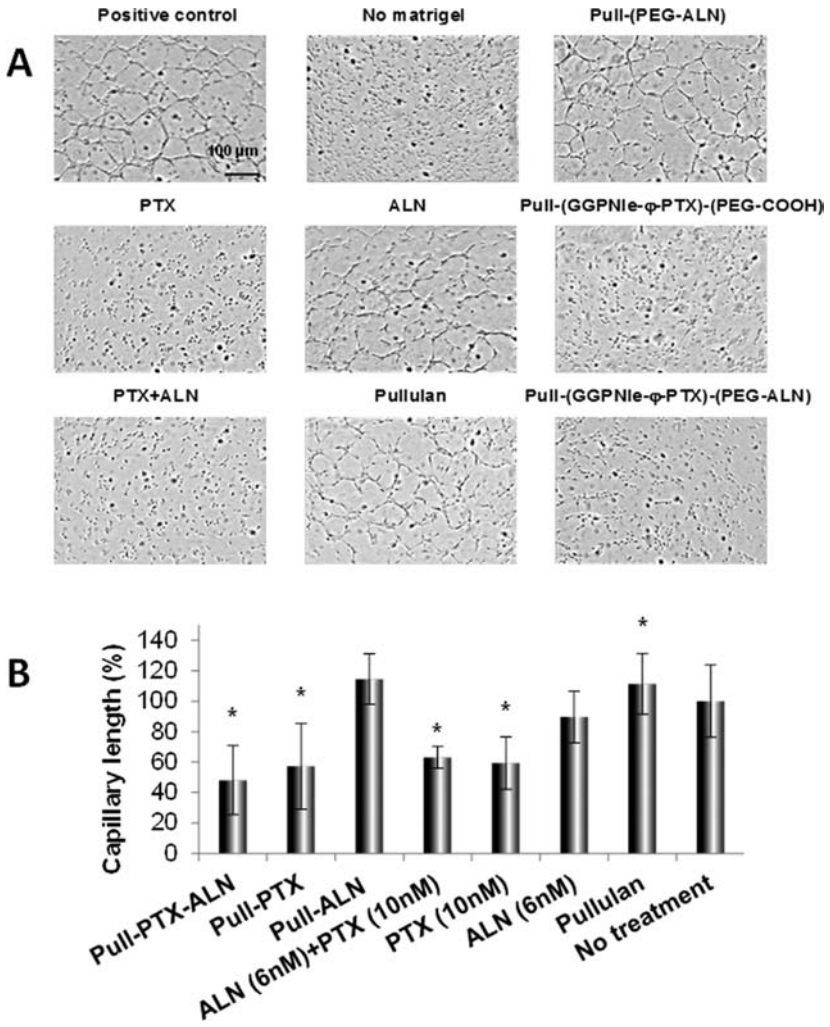


**Figure 8.** Capillary like-tube formation assay: (A) representative images of capillary-like tube structures of HUVEC seeded on Matrigel following treatment; (B) quantitative analysis of the mean length of the tubes. Data represents mean ± SD *$p$ < 0.05. Positive control = no treatment, Negative control = No Matrigel (cannot be quantified).

dictating the biopharmaceutical performance of polymer therapeutics.[40] Under physiological conditions Pull-(GGPNle-$\varphi$-PTX)-(PEG-ALN) was found to form dimensionally homogeneous spherical colloidal structures of about 70 nm, which are suitable for the accumulation in the tumor masses by EPR effect.[41−43] The formation of the supramolecular assemblies at very low bioconjugate concentration, as shown by the low CMC value, can be ascribed to the hydrophobic PTX units that promote the multiple chain association. We hypothesize that the self-assembly of the conjugate yields intramolecule and intermolecule micelles as opposed to solely intermolecule formed by PTX-PEG-ALN.[34] Indeed, Pull-(PEG-ALN) was neither found to form colloidal particles nor reach CMC. Furthermore, the hydrodynamic size of the Pull-(GGPNle-$\varphi$-PTX)-(PEG-ALN) assemblies was found to increase as the pH decreases, supporting that hydrophobic interactions promote the bioconjugate association. As the pH decreases, the content of un-ionized PEG-COOH attached to the polysaccharide increases, yielding to low soluble species that form large size supramolecular structures. As the pH increases, the PEG-COOH ionization increases, which may result in assembly dissociation due to the increased bioconjugate solubility and interchain charge repulsion.

According to its high hydrophilicity and flexibility, the PEG-ALN pending group on the pullulan was expected to be externally exposed on the colloidal surface where it is available for the target recognition, as confirmed by the affinity studies performed by using HAp. The differences between the bioconjugate interactions with HAp observed at pH 5.5 and 7.4 are in agreement with the structural differences observed at various pHs and indicate that the conformational structure of the polymer can affect the polymer/substrate recognition and interaction. At low pH, the polymer is associated in colloidal assemblies and the conjugated PEG-COOH contributes to the interchain association while PEG-ALN is exposed on the surface for interaction with HAp. At higher pH, the assemblies partially dissociate and the ionized PEG-COOH can interfere with the PEG-ALN for the HAp interaction.

The presence of PEG moieties in the bioconjugate has a significant effect on the PTX solubility, which was about 1700-fold higher as compared to the unconjugated drug. The increased solubility eliminates the need for Cremophor EL in the PTX formulation, which is responsible for several side effects.[11] Hemolysis studies showed that Pull-(GGPNle-$\varphi$-PTX)-(PEG-ALN) has higher blood compatibility as compared to formulations containing Cremophor EL.[44] This result demonstrates that the bioconjugate, despite its amphiphilic


DOI: 10.1021/bc500614b
*Bioconjugate Chem.* 2015, 26, 489−501

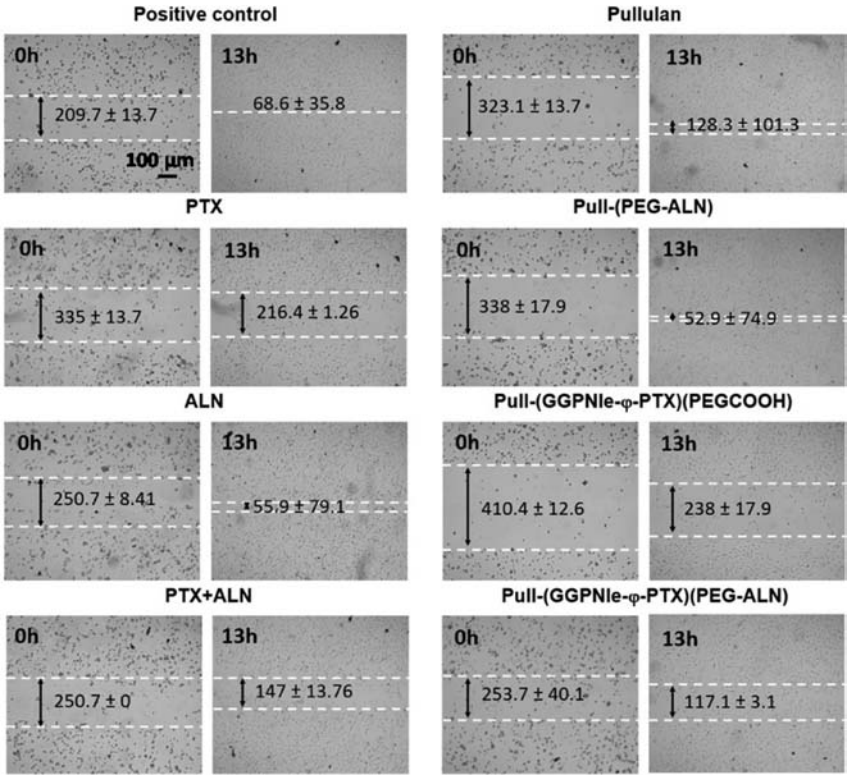


**Figure 9.** Wound healing assay on HUVEC incubated with free PTX, free ALN, Pull, Pull-(GGPNle-$\varphi$-PTX)-(PEG-COOH), Pull-(PEG-ALN), and Pull-(GGPNle-$\varphi$-PTX)-(PEG-ALN) at equivalent concentration of PTX and for 13 h.

properties conferred by the presence of hydrophobic and hydrophilic moieties, (GGPNle-$\varphi$-PTX) and (PEG-ALN)/(PEG-COOH), respectively, does not undergo unspecific cell membrane interaction and cell disruption.

Stability studies showed that under physiological conditions at 37 °C the bioconjugate is chemically and physically stable over more than 8 h, a prerequisite for EPR accumulation in the tumor size that takes place throughout a few hours of circulation in the bloodstream.[45,46] At pH 7.4, neither hydrodynamic size nor size polydispersity changes were observed. Furthermore, with respect to other similar bioconjugates,[19,20] Pull-(GGPNle-$\varphi$-PTX)-(PEG-ALN) did not yield drug release in 24 h. The chemical stability can be ascribed to localization of the (GGPNle-$\varphi$-PTX) module in the core of the assembly that prevents the chemical hydrolysis observed in the case of dendrimeric bioconjugates[19,20] where this module is exposed on the surface. The drug was instead rapidly released in the presence of Cathepsin K under conditions simulating the external lysosomal environment typical of the osteoclast lacunae. The rapid PTX release indicates that the polymeric assemblies have a loose structure, probably conveyed by the PEG-COOH chains also present in the Pull-(GGPNle-$\varphi$-PTX)-(PEG-ALN) derivative, that allows for the Cathepsin K penetration.

The toxicity and biological activity of Pull-(GGPNle-$\varphi$-PTX)-(PEG-ALN) was assessed in vitro by using MDA-MB-231 human mammary adenocarcinoma cells that were in vivo inoculated in mice to isolate an aggressive bone metastases-derived cell population (MDA-MB-231-BM), which simulates the early invasive phase of breast cancer that forms bone metastases. In addition, we used 4T1 murine mammary adenocarcinoma cells, which mimic a stage IV human breast cancer with similar kinetics to the human clinical scenario of bone metastases. When injected in mice, these breast cancer cells spontaneously disseminate tumor cells from the primary tumor to the bone thus making them a good model in breast cancer bone metastasis targeting. Human SAOS-2 and murine K7M2 osteosarcoma cell lines were used as models for primary bone neoplasms.

The cell culture studies showed that Pull-(GGPNle-$\varphi$-PTX)-(PEG-ALN) is about 5−20 times less cytotoxic toward MDA-MB-231-BM, 4T1, and SAOS-2 cells than free PTX, while it was 5 times more active in the case of K7M2. The different antiproliferative activity of Pull-(GGPNle-$\varphi$-PTX)-(PEG-ALN) and PTX can be ascribed to a combination of effects, namely, different cell interaction, uptake pathway, drug availability, and Cathepsin K levels. Actually, the free drug can be rapidly taken up by the cells by passive diffusion,[10] while in the case of the bioconjugates, the drug must be released by Cathepsin K overexpressed by the cancer cells to the culture medium. The in vitro studies showed that the release of PTX by Cathepsin K requires a few hours and takes place at the same rate from Pull-(GGPNle-$\varphi$-PTX)-(PEG-ALN) and Pull-(GGPNle-$\varphi$-PTX)-(PEG-COOH) conjugates. Therefore, the drug uptake is expected to be slower compared with the free drug that rapidly enters the cells. However, Pull-(GGPNle-$\varphi$-PTX)-(PEG-ALN) was significantly more active than the untargeted bioconjugate Pull-(GGPNle-$\varphi$-PTX)-(PEG-COOH) suggesting that ALN promotes the cell interaction and uptake. This hypothesis seems to be confirmed by the wound healing assay performed on MDA-MB-231-BM cells, which simulates tumor cell invasion and metastasis, and by the assays on HUVEC, namely, cell proliferation assay, capillary-like tube assay, and wound healing assay.

The wound healing assay showed that both Pull-(GGPNle-$\varphi$-PTX)-(PEG-ALN) and Pull-(GGPNle-$\varphi$-PTX)-(PEG-


DOI: 10.1021/bc500614b
Bioconjugate Chem. 2015, 26, 489−501

COOH) inhibit cell migration even though the former was much more active than the latter. Therefore, both conjugates seem to be taken up by the cancer cells but the uptake of the derivative bearing ALN is higher. Furthermore, ALN itself is anti-angiogenic and adds synergistic inhibitory activity to the PTX.[34] The assays on HUVEC showed that Pull-(GGPNle-φ-PTX)-(PEG-ALN) retained the PTX anti-angiogenic properties. The activity of the bioconjugate was similar to that observed with PTX, whereas Pull-(GGPNle-φ-PTX)-(PEG-COOH) demonstrated lower anti-angiogenic activity, suggesting that synergism occurs between PTX and ALN. It is important to note that ALN is not released from Pull-(GGPNle-φ-PTX)-(PEG-ALN). Indeed, this bioconjugate was designed to exploit the targeting properties of ALN rather than its anti-angiogenic activity. Nevertheless, the results obtained with HUVEC cells suggest that ALN can also maintain anti-angiogenic activity even when bound to the polymeric structure. It should be noted that the bisphosphonate anti-angiogenic potential and the development of avascular bone necrosis is a desirable effect to decrease tumor vessel ingrowth[18] and maintenance of bone integrity.[34]

## 4. CONCLUSIONS

The present study shows that pullulan derivatives can be properly designed for selective treatment of breast cancer bone metastasis. The efficiency of this class of bioconjugates relies on the combination of various physicochemical and biopharmaceutical features that include solubility, colloidal size that allows for long circulation in the bloodstream and passive accumulation in the tumor tissue, stability under physiological conditions, cell targeting, and selective drug release in the target site. The results reported in this paper show that the pullulan bioconjugate described here possesses the main requisites for pharmaceutical applications, in terms of stability, biocompatibility, and pharmacological activity, which make this product a suitable candidate for enhancing active paclitaxel delivery. The overall results reported here show that Pull-(GGPNle-φ-PTX)-(PEG-ALN) is less active than free PTX. Nevertheless, it possesses significant selectivity conveyed by both targeting agent and cleavable linker that can greatly enhance the in vivo therapeutic performance of PTX. Finally, the studies show that despite the fact that ALN is not conjugated to the scaffold through a releasable bond, it can exert anti-angiogenic activity that synergistically contributes to PTX's activity.[9]

## 5. EXPERIMENTAL PROCEDURES

Fmoc-proline, Fmoc-glycine, and Fmoc-Norleucine-Wang resin (Fmoc-Nle-Wang-R) were purchased from Bachem (Bubendorf, Switzerland). Hydroxybenzotriazole (HOBt) and *N,N,N′,N′*-Tetramethyl-*O*-(1*H*-benzotriazol-1-yl)uronium hexafluorophosphate (HBTU) were obtained from ABI S.r.l (Milan, Italy). Cathepsin K was obtained from Calbiochem (Darmstadt, Germany), alendronate (ALN) from LTBio (Shanghai, China), and paclitaxel (PTX) from LC Laboratories (Woburn, USA). Pullulan (Pull) and all other chemical reagents, including salts, silica gel, trifluoroacetic acid, coupling agents, and deuterated solvents used for NMR spectroscopy analyses and all the solvents of appropriate purity (HPLC or higher degree of purity) were purchased from Sigma-Aldrich (St. Louis, USA), VWR (Milan, Italy), or Carlo Erba (Milan, Italy). α-*t*-Butyloxycarbonylamino-ω-carboxy succinimidyl ester poly(ethylene glycol) (tBoc-NH-PEG-NHS, 3 kDa molecular weight) was purchased from Iris Biotech (Marktredwitz, Germany). Dulbecco's modified Eagle's medium (DMEM), Roswell Park Memorial Institute medium (RPMI 1640), Foetal Bovine Serum (FBS), penicillin, streptomycin, nystatin, L-glutamine, HEPES buffer, sodium pyruvate, and fibronectin were obtained from Biological Industries Ltd. (Kibbutz Beit Haemek, Israel). Growth factor-reduced medium EBM-2 and EGM-2 medium were purchased from Lonza (Switzerland). Matrigel was from BD Biosciences (USA). 3-(4,5-Dimethylthiazol-2-yl)-2,5-diphenyltetrazolium bromide (MTT) was purchased from Sigma-Aldrich (St. Louis, USA). MDA-MB-231-BM human mammary adenocarcinoma (derived from MDA-MB-231), 4T1 murine adenocarcinoma, SAOS-2 human osteosarcoma, and K7M2 murine osteosarcoma cell lines were purchased from American Type Culture Collection (ATCC). Human Umbilical Vein endothelial cells (HUVEC) were obtained from Cambrex (Walkersville, USA).

**5.1. Synthesis of $NH_2$Gly-Gly-Pro-Nle-φ-Paclitaxel ($NH_2$GGPNle-φ-PTX).** All following reactions were performed under nitrogen atmosphere.

*5.1.1. Synthesis of Fmoc-Gly-Gly-Pro-NleOH (Fmoc-GGPNle).* The tetrapeptide Fmoc-Gly-Gly-Pro-NleOH (Fmoc-GGPNle) was obtained by solid phase peptide synthesis (SPPS) using a Wang-Nle-Fmoc resin and standard stepwise Fmoc chemistry.[47] The amino acid coupling of Fmoc-Pro and Fmoc-Gly was carried out in the presence of 5% mol *N,N*-diisopropylethylamine (DIPEA, 4.52 g) in dimethylformaldehyde (DMF, 89.3 g) while the stepwise amino acid deprotection was carried out using 20% mol piperidine (17.4 g, 0.21 mol) in 1-methyl-2-pyrrolidone (NMP, 82.4 g, 0.83 mol). The Wang-Nle-Pro-Gly-Gly-Fmoc solid was finally treated, with a 95% vol/vol trifluoroacetic acid (TFA) in water, for 30 min in the dark. The free tetrapeptide Fmoc-GGPNle was recovered by precipitation into water to yield a white/off-white powder after lyophilization. The purified product was analyzed by mass spectrometry (ESI-TOF, positive mode) and $^1$H NMR spectrometry in $CDCl_3$.

ESI-TOF [*m*/*z*]: 565.3051 $[M+H]^+$ (calcd for $C_{30}H_{36}N_4O_7$: 564.6294). $^1$H NMR: $\delta$ = 0.84 ppm (Nle, 3H, C$\underline{H}_3$), $\delta$ = 8.38 ppm (1H, N$\underline{H}$), 8.05 ppm (1H, N$\underline{H}$), $\delta$ = 7.36 ppm (m, 4H, C$\underline{H}$, Fmoc), $\delta$ = 7.70 ppm (m, 1H + 1H, C$\underline{H}$, Fmoc). $\delta$ = 7.88 ppm (m, 2H,C$\underline{H}$, Fmoc). $\delta$ = 1.27 ppm (m, 4H, C$\underline{H}_2$-C$\underline{H}_2$), $\delta$ = 2.11 ppm (m, 2H, C$\underline{H}_2$).

*5.1.2. Synthesis of Fmoc-GGPNle-benzyl-OH (Fmoc-GGPNle-φ-OH).* Fmoc-GGPNle (100 mg, 177 μmol) was dissolved in 4 mL of 20:80 vol/vol dioxane:THF solvent mixture and cooled to −18 °C. *N*-Methylmorpholine (NMP, 19 μL, 177 μmol) and isobutylchloroformate (28 μL, 212 μmol) were added at once and the reaction was maintained under stirring for 20 min, followed by addition of 4-aminobenzyl alcohol (φ, 32.7 mg, 265 μmol). The reaction was kept at −18 °C for 16 h and then filtered. The filtrate was concentrated under vacuum to yield a yellow viscous product. Fmoc-GGPNle-φ-OH was purified by a two-step silica chromatography protocol using (1) ethyl acetate and (2) 20:80 vol/vol ethyl acetate:acetone. The purification was monitored by TLC. The fractions corresponding to Fmoc-GGPNle-φ-OH were collected and concentrated under vacuum. Fmoc-GGPNle-φ-OH was recovered as a white powder and analyzed by mass spectrometry (ESI-TOF, positive mode).


DOI: 10.1021/bc500614b
Bioconjugate Chem. 2015, 26, 489−501

ESI-TOF [$m/z$]: 670.3291 $[M+H]^+$ (calcd for $C_{37}H_{43}N_5O_7$: 669.7666).

*5.1.3. Synthesis of Fmoc-GGPNle-φ-p-nitrophenyl Ester (Fmoc-GGPNle-φ-pNO$_2$).* A solution of Fmoc-GGPNle-φ-OH (113 mg, 168 μmol) in anhydrous THF (4 mL) was cooled to 0 °C followed by addition of diisopropylethylamine (DIPEA, 117 μL, 674 μmol), *p*-nitrophenyl chloroformate (102 mg, 506 μmol), and a catalytic amount of pyridine (2 μL). The reaction mixture was maintained under stirring at 0 °C for 16 h, concentrated under vacuum, and dissolved in ethyl acetate (5 mL). The organic phase was washed three times with ammonium chloride solution (saturated solution, 3 × 5 mL), dried over sodium sulfate, and finally filtered off. The filtrate was concentrated at low pressure. The purification was carried out by the two-step silica chromatography procedure described above and monitored by TLC. The fractions corresponding to *Fmoc-GGPNle-φ-pNO$_2$* were collected and concentrated under vacuum. *Fmoc-GGPNle-φ-NO$_2$* was recovered as a white powder and analyzed by mass spectrometry (ESI-TOF, positive mode).

ESI-TOF [$m/z$]: 852.3674 $[M{\cdot}H_2O+NH_4)^+$ (calcd for $C_{44}H_{46}N_6O_{11}$: 851.0696).

*5.1.4. Synthesis of NH$_2$GGPNle-φ-PTX.* Fmoc-GGPNle-φ-NO$_2$ (59 mg, 71 μmol) was dissolved in anhydrous THF (4 mL), followed by addition of paclitaxel (PTX, 72 mg, 85 μmol) and dimethylaminopyridine (DMAP, 13 mg, 106 μmol). The reaction was maintained under stirring at room temperature for 8 h and then concentrated under vacuum. The purification was carried out according to the two-step silica chromatography procedure described above and monitored by TLC. The fractions corresponding to Fmoc-GGPNle-φ-PTX were collected, concentrated under vacuum, and analyzed by mass spectrometry (ESI-TOF, positive mode).

ESI-TOF [$m/z$]: 1549.1414 $[M+H]^+$ (calcd for $C_{85}H_{92}N_6O_{22}$: formula weight: 1548.6669.

*5.1.5. Synthesis of NH$_2$GGPNle-φ-PTX.* Fmoc-GGPNle-φ-PTX (93 mg, 90 μmol) was dissolved in dichloromethane (DCM, 4 mL), followed by addition of DMAP (11 mg, 77.4 μmol). The reaction mixture was maintained under stirring at room temperature for 48 h, and monitored by mass spectrometry (ESI-TOF, positive mode). NH$_2$GGPNle-φ-PTX was recovered by precipitation into cold diethyl ether followed by evaporation of solvents under vacuum. The white product was analyzed by mass spectrometry (ESI-TOF, positive mode).

ESI-TOF [$m/z$]: 1328.6470 $[M+H]^+$ (calcd for $C_{70}H_{82}N_6O_{20}$: 1327.4282).

**5.2. Synthesis of NH$_2$PEG-Alendronate (NH$_2$PEG-ALN).** ALN (50 mg, 153.84 μmol) was dissolved in 0.1 M borate buffer, pH 8 (5 mL), followed by addition of tBoc-PEG-NHS (3 kDa, 165 mg, 55 μmol). The reaction mixture was maintained for 5 h under stirring at room temperature, and then the pH was adjusted at 4.5 using 0.2 M HCl. tBoc-PEG-alendronate (tBoc-PEG-ALN) was extracted in DCM (6 × 5 mL), and the organic phase was dried over sodium sulfate and precipitated into cold diethyl ether after filtration. tBoc-PEG-ALN was then dialyzed against water for 2 days and lyophilized. The unconjugated ALN was determined by TNBS test according to the Snyder and Sabocinsky assay.[48] tBoc-PEG-ALN (60 mg, 20 μmol) was dissolved in 1 mL of 50:50 vol/vol trifluoroacetic acid:dichloromethane (TFA/DCM) and the reaction mixture was maintained at room temperature under stirring for 30 min. DCM and TFA were removed under vacuum and NH$_2$-PEG-ALN was recovered by precipitation into diethyl ether to yield a white powder. The content of ALN and PEG in the final product was determined by colorimetric assays.[49,50]

**5.3. Synthesis of Pull-(GGPNle-φ-PTX)-(PEG-ALN), Pull-(GGPNle-φ-PTX)-(PEG-COOH), and Pull-(PEG-ALN).** *5.3.1. Synthesis of Pull-(GGPNle-φ-PTX)-(PEG-ALN).* Oxidized pullulan obtained according to the procedure reported in the literature[29] (100 mg, 22% mol oxidation, 272 μmol aldehyde equiv) was dissolved in dimethyl sulfoxide (DMSO, 8 mL). The pullulan solution was added of NH$_2$GGPNle-φ-PTX (120 mg, 90 μmol) dissolved in DMSO (2 mL) and maintained under stirring at room temperature for 12 h. Sodium triacetoxyborohydride (20 mg, 90 μmol) was added to the reaction mixture, maintained under stirring for 6 h, and then added of NH$_2$PEG-ALN (159 mg, 52 μmol) dissolved in DMSO (1 mL). The reaction mixture was maintained under stirring overnight at room temperature and then sodium borohydride (10 mg, 272 μmol) was added. The reaction mixture was maintained at room temperature overnight under stirring and then was dialyzed against water (4 × 1 L) for 2 days. The product was freeze−dried, washed with methanol (5 × 5 mL), and the residual solvent finally eliminated under vacuum to yield a white/off-white brittle powder. The total PTX content in the final product was determined by UV spectrophotometry at $\lambda$ = 234 nm and the unconjugated PTX by RP-HPLC using a C18 column (Phenomenex Luna C18, 4.6 × 250 mm) isocratically eluted with 45:55 vol/vol ACN:water containing 0.05% TFA. The flow rate was 0.7 mL/min and the UV detector was set at 227 nm. The ALN content was determined as reported above. The conjugated PEG was indirectly calculated by determining the unconjugated PEG in the dialyzed volumes by iodine assay reported above.

*5.3.2. Synthesis of Pull-(GGPNle-φ-PTX)-(PEG-COOH).* Pull-(GGPNle-φ-PTX)-(PEG-COOH) was prepared according to the procedure described in section 5.3.1 except that NH$_2$-PEG-COOH (156 mg, 52 μmol) was used instead of NH$_2$PEG-ALN.

*5.3.3. Synthesis of Pull-(PEG-ALN).* Pull-(PEG-ALN) was synthesized according to the procedure reported in section 5.3.1. NH$_2$PEG-ALN (159 mg, 52 μmol) in DMSO (1 mL) was added to oxidized pullulan (100 mg, 22% mol oxidation, 272 μmol aldehyde equiv) dissolved in DMSO (8 mL), and the reaction mixture was maintained under stirring overnight at room temperature. Subsequently, sodium borohydride (10 mg, 272 μmol) was added to the reaction mixture that was then processed and the product analyzed as reported above.

**5.4. Gel Permeation Chromatography.** Gel permeation chromatography (GPC) was performed using two columns in series: TSK G3000SWXL and TSK G4000SWXL (7.8 × 300 mm, Tosoh) operated on a HPLC system equipped with a refractive index (RI) detector and isocratically eluted using ultrafiltered water at room temperature, at a flow rate of 0.6 mL/min. Molecular weight ($M_w$) and polydispersity ($M_w/M_n$) of native and derivatized pullulan were determined on a calibration curve obtained with pullulan standards (270, 150, 80, 50, 25, 12 kDa).

**5.5. Critical Micelle Concentration (CMC) Determination.** The critical micelle concentration (CMC) of Pull-(GGPNle-φ-PTX)-(PEG-ALN) and Pull-(GGPNle-φ-PTX)-(PEG-COOH) was determined by fluorescence spectroscopy using pyrene as a hydrophobic fluorescent probe.[51] Briefly, Pull-(GGPNle-φ-PTX)-(PEG-ALN) and Pull-(GGPNle-φ-PTX)-(PEG-COOH) samples were prepared by dissolving the


DOI: 10.1021/bc500614b
Bioconjugate Chem. 2015, 26, 489−501

conjugate in 20 mM phosphate buffer, 0.15 M NaCl (PBS), pH 7.4, to yield polymer concentrations in the range of 0.2 to 100 μg/mL. Volumes of 5 μL of 0.18 mM pyrene solution in acetone were added to 750 μL of the polymer solutions and the samples were maintained under gentle shaking at room temperature overnight, protected from the light. The solutions were incubated at 37 °C for 15 min and fluorescence excitation spectra were recorded in the 300 to 360 nm wavelength range with an emission wavelength ($\lambda_{em}$) set at 390 nm using a Jasco FP-6500 Spectrofluorometer. The $I(\lambda_{ex}$ 339 nm$)/I(\lambda_{ex}$ 334 nm) intensity ratios were plotted as a function of the logarithm of the polymer concentration (logC). The CMC was determined from the intersection point of the resulting two curves.

**5.6. Particle Size Analysis.** The particle size and size polydispersity were measured by dynamic light scattering (DLS) using a Malvern Instrument Ltd. Zetasizer Nano ZS (Malvern, UK). Pull-(GGPNle-φ-PTX)-(PEG-ALN) samples were analyzed at concentrations of 1 mg/mL in 20 mM sodium acetate, pH 5.5, PBS, pH 7.4, and Milli-Q water.

**5.7. Transmision Electron Microscopy.** Transmission electron microscopic analyses were carried out using a Tecnai G2 microscope (FEI). The bioconjugate (1.5 mg/mL) in PBS at pH 7.4 was deposited on an homemade carbon coated copper grid. The excess volume was removed with filter paper and the samples were negatively stained with 1% uranyl acetate dissolved in distilled water and analyzed.

**5.8. Stability Studies.** Pull-(GGPNle-φ-PTX)-(PEG-ALN) and Pull-(GGPNle-φ-PTX)-(PEG-COOH) solutions (75 μM PTX equivalent, 3 mL) in 20 mM sodium acetate, pH 5.5, or in PBS, pH 7.4, were introduced into 14 kDa cutoff dialysis bags, placed in 50 mL of the corresponding medium and maintained at 37 °C. At fixed time intervals, 60 μL samples were withdrawn from the dialysis bag. Then, samples were analyzed spectrophotometrically and chromatographically for the determination of ALN and PTX. The assay was performed three times.

**5.9. Drug Release Studies.** Samples were prepared by mixing 303 μL of 2.5 mM L-cysteine, 146 μL of 5 mM ethylenediaminetetraacetic acid (EDTA), and 84 μL of 5 mM DL-dithiothreitol (DTT) solutions. All stock solutions were prepared in 50 mM sodium acetate, 100 mM NaCl, pH 5.5. The samples were warmed up at 37 °C for 5 min followed by addition of 162 μL of 150 nM Cathepsin K. Finally, 305 μL of 75 μM PTX equivalent of Pull-(GGPNle-φ-PTX)-(PEG-ALN) solutions in acetate buffer were added to the samples. The mixtures were incubated at 37 °C and aliquots of 75 μL were withdrawn after 0, 15, 30, 45, 60, 120, 240, 480, and 1220 min and analyzed by RP-HPLC as reported above (2.5). The assay was repeated three times.

**5.10. Hydroxyapatite Binding Assay.** Pull-(GGPNle-φ-PTX)-(PEG-ALN), Pull-(GGPNle-φ-PTX)-(PEG-COOH) (3 mg/mL, 75 μM PTX equivalent), and free ALN solutions in 20 mM sodium acetate buffer, 0.15 M NaCl, pH 5.5, or in PBS, pH 7.4, were incubated under stirring at 37 °C for 15 min. Hydroxyapatite (30 equiv) was then added to each solution and the suspensions were maintained under stirring at 37 °C. At scheduled times, the suspensions were centrifuged for 10 min at 5000 rpm and 60 μL of the supernatant were withdrawn and spectrophotometrically and chromatographically analyzed for PTX and ALN determination. The binding of the conjugate to hydroxyapatite was calculated as follows:

$$\%\ \text{binding} = [(\text{sample concentration without hydroxyapatite} - \text{sample concentration with hydroxyapatite})] / [\text{sample concentration without hydroxyapatite}] \times 100$$

**5.11. Cell Culture.** MDA-MB-231-BM cells were cultured in DMEM supplemented with 10% FBS, 100 μg/mL penicillin, 100 U/mL streptomycin, 12.5 U/mL nystatin, and 2 mM L-glutamine. SAOS-2 and K7M2 cells were cultured in DMEM supplemented with 10% FBS, 100 μg/mL penicillin, 100 U/mL streptomycin, 12.5 U/mL nystatin, 2 mM L-glutamine, and 1 mM sodium pyruvate. 4T1 cells were cultured in RPMI 1640 supplemented with 10% FBS, 100 μg/mL penicillin, 100 U/mL streptomycin, 12.5 U/mL Nystatin, 2 mM L-glutamine, 10 mM HEPES buffer, and 1 mM sodium pyruvate. Human umbilical vein endothelial cells (HUVEC) were obtained from Cambrex (Walkersville, USA) and grown according to manufacturer's protocol in EGM-2 medium (Cambrex). All cells were grown at 37 °C, 5% $CO_2$.

**5.12. Cell Proliferation Assays.** 4T1 ($4 \times 10^3$ cells/well) cells, K7M2 ($1.5 \times 10^3$ cells/well) cells, and HUVEC ($1.5 \times 10^3$ cells/well) were plated onto 24-well plates in RPMI, DMEM/pyruvate, and growth factor reduced media EBM-2, respectively, supplemented with 10% FBS. Following 24 h incubation at 37 °C and 5% $CO_2$, the medium was replaced with 10% FBS supplemented RPMI and EGM-2 correspondingly.

MDA-MB-231-BM cells ($5 \times 10^3$ cells/well) and SAOS-2 cells ($2 \times 10^3$ cells/well) were plated onto 96-well plates in DMEM and DMEM/pyruvate, respectively, supplemented with 5% FBS. After 24 h incubation at 37 °C and 5% $CO_2$ atmosphere, the medium was replaced by a 10% FBS supplemented DMEM and DMEM/pyruvate correspondingly.

Cells were challenged with (1) free PTX; (2) free ALN; (3) Pull; (4) Pull-(GGPNle-φ-PTX)-(PEG-COOH); (5) Pull-(PEG-ALN); (6) Pull-(GGPNle-φ-PTX)-(PEG-ALN) at serial concentrations in culture medium. Following 72 h incubation, 4T1, K7M2, and HUVEC cells were counted by Coulter counter and the MDA-MB-231-BM and SAOS-2 cell viability was measured by the Thiazolyl blue formazan (MTT) method. Briefly, 20 μL of a 5 mg/mL MTT solution in 20 mM PBS, pH 7.4, were added to each well containing cells grown in 100 μL medium. After 5 h incubation at 37 °C, 5% $CO_2$, the medium was replaced by 200 μL DMSO. After dissolution of the crystals, the 96-well plate was determined by UV spectrophotometry at $\lambda$ = 565 nm.

**5.13. In Vitro Tube Formation Assay.** Matrigel basement membrane (50 μL/well) was layered onto each well of ice-cooled 24-well plates and allowed to polymerize for 30 min at 37 °C. After Matrigel solidification, HUVEC cells in EGM-2 medium were treated with (1) 10 nM PTX; (2) a combination of 10 nM PTX and 5.0 nM ALN; (3) 5.0 nM ALN; (4) Pull; (5) 5.0 nM ALN equivalent Pull-(PEG-ALN); (6) 10 nM PTX equivalent Pull-(GGPNle-φ-PTX)-(PEG-COOH); (7) 10 nM PTX and 5.0 nM ALN equivalent Pull-(GGPNle-φ-PTX)-(PEG-ALN) and seeded onto the coated plates. After 8 h incubation at 37 °C and 5% $CO_2$, wells were imaged using Nikon TE2000E inverted microscope integrated with Nikon DS5 cooled CCD camera by 4× objective, bright field technique. The tube networks were quantified by image analysis using *ImageJ* software.



DOI: 10.1021/bc500614b
*Bioconjugate Chem.* 2015, 26, 489−501

**5.14. Wound Healing Assay (Scratch Test).** HUVEC were plated onto 6-well plates ($5 \times 10^5$ cells/well), MDA-MB-231-BM cells were plated onto 6-well plates ($4 \times 10^5$ cells/well), and incubated for 24 h, at 37 °C, 5% $CO_2$. After this time, the confluent monolayer was scratched by a pipet tip, rinsed with sterile PBS, pH 7.4, to remove detached cells, and fresh medium was added. Digital images of cells were taken immediately after scratching ($t = 0$). The cells were then treated with (1) 10 nM PTX; (2) Combination of 10 nM PTX and 5.0 nM ALN; (3) 5.0 nM ALN; (4) 20 nM Pull; (5) 5 nM ALN-equivalent Pull-(PEG-ALN); (6) 10 nM PTX-equivalent Pull-(GGPNle-φ-PTX)-(PEG-COOH); (7) 10 nM PTX and 5 nM ALN equivalent Pull-(GGPNle-φ-PTX)-(PEG-ALN). After 13 h incubation for HUVEC and 24 h incubation for MDA-MB-231-BM, the distance between cells in the scratched area (migration) was evaluated using *ImageJ* software.

**5.15. Red Blood Cells Lysis Assay.** Rat Blood Cells (RBC) were obtained from whole rat blood, diluted 1:1 with PBS, pH 7.4, mixed for 10 s, incubated for 2 min at room temperature and finally centrifuged at 1000 rpm for 5 min at 4 °C. The supernatant was discarded and the seeded cells washed three times with PBS, pH 7.4. RBC dispersion in PBS, pH 7.4 (2% w/vol) was incubated for 1 h at 37 °C with serial dilutions in PBS of (1) PTX and ALN in Cremophor EL; (2) PTX and ALN-equivalent concentrations of Pull-(GGPNle-φ-PTX)-(PEG-ALN); (3) 70 kDa Dextran (negative control); (4) 1 w/vol Triton X100 (1st positive control); (5) poly-(ethylenimine) (PEI, second positive control). The samples were centrifuged for 7 min at 3000 rpm and the absorbance of the supernatant was measured at 550 nm by using a microplate reader. The results were expressed as percent of hemoglobin released relative to the positive control.

**5.16. Statistical Methods.** In vitro data are expressed as mean ± SD (standard deviation). Statistical significance was determined using an unpaired $t$ test. $P < 0.05$ was considered statistically significant. All statistical tests were two-sided.

## ■ ASSOCIATED CONTENT

### Supporting Information

Chemical structure of Pull-(PEG-ALN) and Pull-(GGPNle-φ-PTX)-(PEG-COOH) (Scheme SI1). Synthesis scheme of $NH_2$GGPNle-φ-PTX (Scheme SI2). Mass and $^1$H NMR spectra of Fmoc-GGPNleCOOH (Figures SI1 and SI2) and mass spectra of Fmoc-GGPNle-φ-OH, Fmoc-GGPNle-φ-p$NO_2$ and $NH_2$GGPNle-φ-PTX (Figures SI3, SI4, and SI5). RP-HPLC elution profile of $NH_2$GGPNle-φ-PTX (Figure SI6). Synthesis scheme of $NH_2$PEG-ALN. (Scheme SI3). Synthesis scheme of Pull-(GGPNle-φ-PTX)(PEG-ALN) (Scheme SI4). RP-HPLC chromatograms of native Pullulan, PTX and Pull-(GGPNle-φ-PTX)(PEG-ALN) (Figure SI7). Size distribution profiles of Pull-(GGPNle-φ-PTX)(PEG-ALN) in PBS pH5.5, water and PBS pH 7.4 (Figure SI8). Pyrene fluorescence profile [I($\lambda_{ex}$ 338 nm)/I($\lambda_{ex}$ 334 nm)] as a function of Pull-(GGPNle-φ-PTX)(PEG-ALN) concentration (Figure SI9). Enlarged images of Figure 6 showing the morphology of the MDA-MB-231-BM cells (Figure SI10), enlarged images of Figure 8A (Figure SI11) showing the HUVEC after treatment for the capillary-like tube formation assay and enlarged images of Figure 9 (Figure SI12) showing the morphology of the HUVEC after wound healing assay. This material is available free of charge via the Internet at http://pubs.acs.org.

## ■ AUTHOR INFORMATION


### Corresponding Author

*E-mail: paolo.caliceti@unipd.it.


### Notes

The authors declare no competing financial interest.

## ■ ACKNOWLEDGMENTS

We acknowledge the CARIPARO Foundation Foreign PhD Project 2010, the University of Padova (Ex-60%, C98C13001480005) and the Ministry of Science, Technology and Space of Israel (MOST) and the Directorate General for Political and Security Affairs of the Ministry of Foreign Affairs, Italy scientific cooperation for the financial support (GYN-MIR).

## ■ REFERENCES

(1) Colleoni, M., O'Neill, A., Goldhirsch, A., Gelber, R. D., Bonetti, M., Thurlimann, B., Price, K. N., Castiglione-Gertsch, M., Coates, A. S., Lindtner, J., et al. (2000) Identifying breast cancer patients at high risk for bone metastases. *J. Clin. Oncol. 18*, 3925−35.

(2) Weilbaecher, K. N., Guise, T. A., and McCauley, L. K. (2011) Cancer to bone: a fatal attraction. *Nat. Rev. Cancer 11*, 411−425.

(3) Piccoli, A. (2014) Breast cancer bone metastases: an orthopedic emergency. *J. Orthopedic Traumatology 15*, 143−144.

(4) Uludag, H. (2002) Bisphosphonates as a foundation of drug delivery to bone. *Curr. Pharm. Des. 8*, 1929−44.

(5) Rosen, L. S., Gordon, D., Tchekmedyian, N. S., Yanagihara, R., Hirsh, V., Krzakowski, M., Pawlicki, M., de Souza, P., Zheng, M., Urbanowitz, G., et al. (2004) Long-term efficacy and safety of zoledronic acid in the treatment of skeletal metastases in patients with nonsmall cell lung carcinoma and other solid tumors: a randomized, Phase III, double-blind, placebo-controlled trial. *Cancer 100*, 2613−2621.

(6) Morris, G. J., and Mitchell, E. P. (2007) Bisphosphonate therapy for women with breast cancer and at high risk for osteoporosis. *J. Natl. Med. Assoc. 99*, 35−45.

(7) Hillner, B. E., Ingle, J. N., Chlebowski, R. T., Gralow, J., Yee, G. C., Janjan, N. A., Cauley, J. A., Blumenstein, B. A., Albain, K. S., Lipton, A., et al. (2003) American Society of Clinical Oncology 2003 Update on the Role of Bisphosphonates and Bone Health Issues in Women With Breast Cancer. *J. Clin. Oncol. 21*, 4042−4057.

(8) Russell, R. G. G. (2011) Bisphosphonates: The first 40 years. *Bone 49*, 2−19.

(9) Jagdev, S. P., Coleman, R. E., Shipman, C. M., Rostami-H, A., and Croucher, P. I. (2001) The bisphosphonate, zoledronic acid, induces apoptosis of breast cancer cells: evidence for synergy with paclitaxel. *Br. J. Cancer 84*, 1126−1134.

(10) Rose, W. C. (1992) Taxol: a review of its preclinical in vivo antitumor activity. *Anti-Cancer Drugs 3*, 311−322.

(11) Kiss, L., Walter, F. R., Bocsik, A., Veszelka, S., Ózsvári, B., Puskás, L. G., Szabó-révész, P., and Deli, M. A. (2013) Kinetic analysis of the toxicity of pharmaceutical excipients cremophor EL and RH40 on endothelial and epithelial cells. *J. Pharm. Sci. 102*, 1173−1181.

(12) Ma, P., and Mumper, R. J. (2013) Paclitaxel nano-delivery systems: a comprehensive review. *J. Nanomed. Nanotechnol. 4*, 1000164.

(13) Nehate, C., Jain, S., Saneja, A., Khare, V., Alam, N., Dubey, R., and Gupta, P. N. (2014) Paclitaxel formulations: challenges and novel delivery options. *Curr. Drug Delivery 11*, 666−86.

(14) Eldar-Boock, A., Miller, K., Sanchis, J., Lupu, R., Vicent, M. J., and Satchi-Fainaro, R. (2011) Integrin-assisted drug delivery of nano-scaled polymer therapeutics bearing paclitaxel. *Biomaterials 32*, 3862−3874.

(15) Singer, J. W. (2005) Paclitaxel poliglumex (XYOTAX, CT-2103): a macromolecular taxane. *J. Controlled Release 109*, 120−6.

(16) Von Hoff, D. D., Ervin, T., Arena, F. P., Chiorean, E. G., Infante, J., Moore, M., Seay, T., Tjulandin, S. A., Ma, W. W., Saleh, M. N., et al.



DOI: 10.1021/bc500614b
*Bioconjugate Chem.* 2015, 26, 489−501

(2013) Increased survival in pancreatic cancer with nab-paclitaxel plus gemcitabine. *New Engl. J. Med. 369*, 1691−703.
(17) Uludag, H., Kousinioris, N., Gao, T., and Kantoci, D. (2000) Bisphosphonate conjugation to proteins as a means to impart bone affinity. *Biotechnol. Prog. 16*, 258−267.
(18) Pabst, A. M., Ziebart, T., Ackermann, M., Konerding, M. A., and Walter, C. (1996) Bisphosphonates' antiangiogenic potency in the development of bisphosphonate-associated osteonecrosis of the jaws: influence on microvessel sprouting in an in vivo 3D Matrigel assay. *Biol. Pharm. Bull. 19*, 1026−1031.
(19) Miller, K., Erez, R., Segal, E., Shabat, D., and Satchi-Fainaro, R. (2009) Targeting bone metastases with a bispecific anticancer and antiangiogenic polymer-alendronate-taxane conjugate. *Angew. Chem., Int. Ed. 48*, 2949−54.
(20) Miller, K., Eldar-Boock, A., Polyak, D., Segal, E., Benayoun, L., Shaked, Y., and Satchi-Fainaro, R. (2011) Antiangiogenic antitumor activity of HPMA copolymer-paclitaxel-alendronate conjugate on breast cancer bone metastasis mouse model. *Mol. Pharmaceutics 8*, 1052−62.
(21) Saravanakumar, G., Park, J. H., Kim, K., and Kwon, I. C. (2011) Polysaccharide-Based Drug Conjugates for Tumor Targeting, in *Drug Delivery in Oncology*, pp 701−746, Wiley-VCH Verlag GmbH & Co. KGaA.
(22) Rose, A. A. N., and Siegel, P. M. (2009) Emerging therapeutic targets in breast cancer bone metastasis. *Future Oncol. 6*, 55−74.
(23) Leathers, T. D. (2003) Biotechnological production and applications of pullulan. *Appl. Microbiol. Biotechnol. 62*, 468−73.
(24) Lee, S. J., Hong, G. Y., Jeong, Y. I., Kang, M. S., Oh, J. S., Song, C. E., and Lee, H. C. (2012) Paclitaxel-incorporated nanoparticles of hydrophobized polysaccharide and their antitumor activity. *Int. J. Pharm. 433*, 121−8.
(25) Paranjpe, P. V., Chen, Y., Kholodovych, V., Welsh, W., Stein, S., and Sinko, P. J. (2004) Tumor-targeted bioconjugate based delivery of camptothecin: design, synthesis and in vitro evaluation. *J. Controlled Release 100*, 275−292.
(26) Haratake, M., Matsumoto, S., Ono, M., and Nakayama, M. (2008) Nanoparticulate glutathione peroxidase mimics based on selenocystine−pullulan conjugates. *Bioconjugate Chem. 19*, 1831−1839.
(27) Scomparin, A., Salmaso, S., Bersani, S., Satchi-Fainaro, R., and Caliceti, P. (2011) Novel folated and non-folated pullulan bioconjugates for anticancer drug delivery. *Eur. J. Pharm. Sci. 42*, 547−58.
(28) Everts, V., and Beertsen, W. (2005) External lysosomes: the osteoclast and its unique capacities to degrade mineralised tissues, in *Lysosomes* (Saftig, P., Ed.) pp 144−155, Chapter 12, Springer Science, New York.
(29) Bruneel, D., and Schacht, E. (1993) Chemical modification of pullulan: 1. Periodate oxidation. *Polymer 34*, 2628−2632.
(30) Goldspiel, B. R. (1997) Clinical overview of the taxanes. *Pharmacotherapy 17*, 110S−125S.
(31) Jasmin, C., Capanna, R., Coia, L., Coleman, R., and Saillant, G. (2005) *Textbook of Bone Metastases*, Wiley.
(32) Lijana, R. C., and Williams, M. C. (1987) Reduction of hemolytic blood damage with dextran. *AIChE 33*.
(33) Cerda-Cristerna, B. I., Flores, H., Pozos-Guillén, A., Pérez, E., Sevrin, C., and Grandfils, C. (2011) Hemocompatibility assessment of poly(2-dimethylamino ethylmethacrylate) (PDMAEMA)-based polymers. *J. Controlled Release 153*, 269−277.
(34) Miller, K., Clementi, C., Polyak, D., Eldar-Boock, A., Benayoun, L., Barshack, I., Shaked, Y., Pasut, G., and Satchi-Fainaro, R. (2013) Poly(ethylene glycol)−paclitaxel−alendronate self-assembled micelles for the targeted treatment of breast cancer bone metastases. *Biomaterials 34*, 3795−3806.
(35) de Groot, F. M. H., Loos, W. J., Koekkoek, R., van Berkom, L. W. A., Busscher, G. F., Seelen, A. E., Albrecht, C., de Bruijn, P., and Scheeren, H. W. (2001) Elongated multiple electronic cascade and cyclization spacer systems in activatible anticancer prodrugs for enhanced drug release. *J. Org. Chem. 66*, 8815−8830.
(36) Carl, P. L., Chakravarty, P. K., and Katzenellenbogen, J. A. (1981) A novel connector linkage applicable in prodrug design. *J. Med. Chem. 24*, 479−480.
(37) LoPachin, R. M., and Gavin, T. (2014) Molecular mechanisms of aldehyde toxicity: a chemical perspective. *Chem. Res. Toxicol. 27*, 1081−1091.
(38) Abdel-Magid, A. F., Carson, K. G., Harris, B. D., Maryanoff, C. A., and Shah, R. D. (1996) Reductive amination of aldehydes and ketones with sodium triacetoxyborohydride. Studies on direct and indirect reductive amination procedures. *J. Org. Chem. 61*, 3849−3862.
(39) Johnson, M. R., and Rickborn, B. (1970) Sodium borohydride reduction of conjugated aldehydes and ketones. *J. Org. Chem. 35*, 1041−1045.
(40) Gimenez, V., James, C., Arminan, A., Schweins, R., Paul, A., and Vicent, M. J. (2012) Demonstrating the importance of polymer-conjugate conformation in solution on its therapeutic output: Diethylstilbestrol (DES)-polyacetals as prostate cancer treatment. *J. Controlled Release 159*, 290−301.
(41) Bae, Y. H., and Park, K. (2011) Targeted drug delivery to tumors: Myths, reality and possibility. *J. Controlled Release 153*, 198−205.
(42) Kong, G., Braun, R. D., and Dewhirst, M. W. (2000) Hyperthermia enables tumor-specific nanoparticle delivery: effect of particle size. *Cancer Res. 60*, 4440−5.
(43) Amiji, M. M. (2006) *Nanotechnology for Cancer Therapy*; Taylor & Francis.
(44) Vader, P., Fens, M. H., Sachini, N., van Oirschot, B. A., Andringa, G., Egberts, A. C., Gaillard, C. A., Rasmussen, J. T., van Wijk, R., van Solinge, W. W., et al. (2013) Taxol((R))-induced phosphatidylserine exposure and microvesicle formation in red blood cells is mediated by its vehicle Cremophor((R)) EL. *Nanomedicine (London) 8*, 1127−35.
(45) Markovsky, E., Baabur-Cohen, H., Eldar-Boock, A., Omer, L., Tiram, G., Ferber, S., Ofek, P., Polyak, D., Scomparin, A., and Satchi-Fainaro, R. (2012) Administration, distribution, metabolism and elimination of polymer therapeutics. *J. Controlled Release 161*, 446−460.
(46) Duncan, R. (2003) The dawning era of polymer therapeutics. *Nat. Rev. Drug Discovery 2*, 347−360.
(47) Merrifield, R. B. (1963) Solid phase peptide synthesis. I. The synthesis of a tetrapeptide. *J. Am. Chem. Soc. 85*, 2149.
(48) Snyder, S. L., and Sobocinski, P. Z. (1975) An improved 2,4,6-trinitrobenzenesulfonic acid method for the determination of amines. *Anal. Biochem. 64*, 284−288.
(49) Kuljanin, J., Janković, I., Nedeljković, J., Prstojević, D., and Marinković, V. (2002) Spectrophotometric determination of alendronate in pharmaceutical formulations via complex formation with Fe(III) ions. *J. Pharm. Biomed. Anal. 28*, 1215−1220.
(50) Skoog, B. (1979) Determination of polyethylene glycols 4000 and 6000 in plasma protein preparations. *Vox Sanguinis 37*, 345−349.
(51) Goddard, E. D., Turro, N. J., Kuo, P. L., and Ananthapadmanabhan, K. P. (1985) Fluorescence probes for critical micelle concentration determination. *Langmuir 1*, 352−355.


DOI: 10.1021/bc500614b
*Bioconjugate Chem.* 2015, 26, 489−501